Electroweak Corrections to $B_{s,d} \to \ell^+\ell^-$

Christoph Bobeth,[1, 2, *] Martin Gorbahn,[1, 3, †] and Emmanuel Stamou[1, 2, 4, ‡]

[1]*Excellence Cluster Universe, Technische Universität München, D–85748 Garching, Germany*
[2]*Institute for Advanced Study, Lichtenbergstrasse 2a,*
Technische Universität München, D–85748 Garching, Germany
[3]*Department of Mathematical Sciences, University of Liverpool, Liverpool L69 3BX, United Kingdom*
[4]*Department of Particle Physics and Astrophysics,*
Weizmann Institute of Science, Rehovot 76100, Israel

We calculate the full two-loop electroweak matching corrections to the operator governing the decay $B_q \to \ell^+\ell^-$ in the Standard Model. Their inclusion removes an electroweak scheme and scale uncertainty of about $\pm 7\%$ of the branching ratio. Using different renormalization schemes of the involved electroweak parameters, we estimate residual perturbative electroweak and QED uncertainties to be less than $\pm 1\%$ at the level of the branching ratio.

I. INTRODUCTION

The rare decays of $B_q \to \ell^+\ell^-$ with $q = d, s$ and $\ell = e, \mu, \tau$ are helicity suppressed in the Standard Model (SM) and can be predicted with high precision, which turns them into powerful probes of nonstandard interactions. In November 2012, LHCb [1] reported first experimental evidence of the decay $B_s \to \mu^+\mu^-$ with a signal significance of $3.5\,\sigma$ and the time integrated and CP-averaged branching ratio

$$\overline{\mathrm{Br}}(B_s \to \mu^+\mu^-) = \left(3.2^{+1.4}_{-1.2}(\mathrm{stat})^{+0.5}_{-0.3}(\mathrm{sys})\right) \cdot 10^{-9}, \quad (1)$$

well in agreement with SM predictions. More recently, the signal significance was raised to $4.0\,\sigma$ after analyzing the currently available data set of 1 fb^{-1} at $\sqrt{s} = 7$ TeV and 2 fb^{-1} at $\sqrt{s} = 8$ TeV, with the result [2]

$$\overline{\mathrm{Br}}(B_s \to \mu^+\mu^-) = \left(2.9^{+1.1}_{-1.0}(\mathrm{stat})^{+0.3}_{-0.1}(\mathrm{sys})\right) \cdot 10^{-9}. \quad (2)$$

CMS confirmed this independently utilizing the complete data set of 5 fb^{-1} at $\sqrt{s} = 7$ TeV and 20 fb^{-1} at $\sqrt{s} = 8$ TeV [3] obtaining

$$\overline{\mathrm{Br}}(B_s \to \mu^+\mu^-) = \left(3.0^{+0.9}_{-0.8}(\mathrm{stat})^{+0.6}_{-0.4}(\mathrm{sys})\right) \cdot 10^{-9} \quad (3)$$

and the slightly better signal significance of $4.3\,\sigma$.

The large decay width difference $\Delta\Gamma_s$ of the B_s system implies that the instantaneous branching ratio at time $t = 0$, $\mathrm{Br}^{[t=0]}(B_q \to \ell^+\ell^-)$, deviates from $\overline{\mathrm{Br}}$. Neglecting for a moment cuts on the lifetime in the experimental determination of $\overline{\mathrm{Br}}$, the fully time-integrated and the instantaneous branching ratios are related in the SM as [4]

$$\overline{\mathrm{Br}} = \frac{\mathrm{Br}^{[t=0]}}{1 - y_q}, \quad \text{where} \quad y_q = \frac{\Delta\Gamma_q}{2\Gamma_q}. \quad (4)$$

LHCb has measured $y_s = 0.088 \pm 0.014$ [5, 6] and established a SM-like sign for $\Delta\Gamma_s$ [7]. By 2018, the experimental accuracy in $\overline{\mathrm{Br}}$ is expected to reach $0.5 \cdot 10^{-9}$ and

with 50 fb^{-1} $0.15 \cdot 10^{-9}$ [8], the latter corresponding to the level of about 5% error with respect to the current central value. Results of comparable precision may be expected from CMS, and perhaps also from ATLAS.

Motivated by the experimental prospects, this work presents a complete calculation of the next-to-leading (NLO) electroweak (EW) matching corrections in the SM, supplemented with the effects of the QED renormalization group evolution (RGE). Thereby, we remove a sizable uncertainty which has often been neglected in the past and became one of the major theoretical uncertainties after the considerable shrinking of hadronic uncertainties from recent progress in lattice QCD.

After decoupling the heavy degrees of freedom of the SM – the top quark, the weak gauge bosons and the Higgs boson – at lowest order in EW interactions, the decay $B_q \to \ell^+\ell^-$ is governed by an effective $\Delta B = 1$ Lagrangian

$$\mathcal{L}_{\mathrm{eff}} = V_{tb} V_{tq}^* \mathcal{C}_{10} P_{10} + \mathcal{L}^{(5)}_{\mathrm{QCD} \times \mathrm{QED}} + \mathrm{h.c.} \quad (5)$$

with a single operator $P_{10} = [\bar{q}_L \, \gamma_\mu \, b_L][\bar{\ell} \, \gamma^\mu \gamma_5 \, \ell]$ and its Wilson coefficient $\mathcal{C}_{10}$, as well as the QCD×QED interactions of leptons and five light quark flavors. V_{ij} denotes the relevant elements of the Cabibbo-Kobayashi-Maskawa (CKM) quark mixing matrix. Here we deviate from the usual convention to factor out combinations of EW parameters[1], such as Fermi's constant, G_F, the QED fine structure constant, α_e, the W-boson mass, M_W, or the sine of the weak mixing angle $s_W \equiv \sin(\theta_W)$. The most common normalizations are

$$\mathcal{C}_{10} = \frac{4 G_F}{\sqrt{2}} c_{10}, \qquad \mathcal{C}_{10} = \frac{G_F^2 M_W^2}{\pi^2} \widetilde{c}_{10}, \quad (6)$$

with the LO Wilson coefficients

$$c_{10} = -\frac{\alpha_e}{4\pi} \frac{Y_0(x_t)}{s_W^2}, \qquad \widetilde{c}_{10} = -Y_0(x_t). \quad (7)$$

---

* christoph.bobeth@ph.tum.de
† martin.gorbahn@liverpool.ac.uk
‡ emmanuel.stamou@weizmann.ac.il

---

[1] Since we shall not vary the EW renormalization scheme of the CKM factor $V_{tb} V_{tq}^*$, we prefer to keep it as a prefactor, to have a universal $\mathcal{C}_{10}$ for both $q = d, s$.

They depend on the gauge-independent function Y_0 [9], where $x_t = (M_t/M_W)^2$ denotes the ratio of top-quark to W-boson masses. We will frequently refer to the choice c_{10} and $\widetilde{c}_{10}$ as the "single-G_F" and "quadratic-G_F" normalization, respectively. The former choice is the standard convention of the $\Delta B = 1$ effective theory in the literature, whereas the latter choice removes the dependence on α_e and s_W in favor of G_F and M_W [10]. At lowest order in the EW interactions both normalizations may be considered equivalent due to the tree-level relation $G_F = \pi\alpha_e/(\sqrt{2}M_W^2 s_W^2)$. In practice, however, large differences arise once numerical input for the EW parameters is used that corresponds to different renormalization schemes. For example, a noticeable 7% change of the branching ratio is caused by choosing $s_W^2 = 0.2231$ in the on-shell scheme instead of $s_W^2 = 0.2314$ in the $\overline{\text{MS}}$ scheme with the numerical values taken from Ref. [11]. At higher orders in EW couplings, the analytic form of $\mathcal{C}_{10}$ depends on the choice of normalization as well as the EW renormalization scheme of the involved parameters. Especially the power of G_F affects the matching, whereas the choice of EW renormalization scheme implies different finite counterterms for the parameters. Thereby, the overall numerical differences among the different choices of normalizations and EW renormalization schemes become much smaller, removing the large uncertainty present at lowest order.

The instantaneous branching ratio takes the form

$$\text{Br}^{[t=0]}(B_q \to \ell^+\ell^-) = \mathcal{N}\left|\mathcal{C}_{10}\right|^2, \qquad (8)$$

with the normalization factor

$$\mathcal{N} = \frac{\tau_{B_q} M_{B_q}^3 f_{B_q}^2}{8\,\pi} |V_{tb}V_{tq}^*|^2 \frac{m_\ell^2}{M_{B_q}^2} \sqrt{1 - 4\,m_\ell^2/M_{B_q}^2}. \quad (9)$$

It exhibits the helicity suppression due to the lepton mass m_ℓ and depends on the lifetime τ_{B_q} and the mass M_{B_q} of the B_q meson. Moreover, a single hadronic parameter enters, the B_q decay constant f_{B_q},

$$\langle 0|\bar{q}\,\gamma_\mu\gamma_5\,b|\bar{B}_q(p)\rangle = if_{B_q}p_\mu. \qquad (10)$$

It is nowadays subject to lattice calculations with errors at a few percent level, eliminating this previously major source of uncertainty [12–15]. The uncertainties due to f_{B_q}, τ_{B_q} and y_q approach a level of below 3% [16] in $\overline{\text{Br}}$. Concerning perturbative uncertainties, the strong dependence of $\mathcal{C}_{10}$ on the choice of the renormalization scheme for M_t is removed when including the NLO QCD contribution in the strong coupling α_s [17–20]. So far the full NLO EW corrections have not been calculated and in this work we close this gap as previously done for the analogous corrections to $s \to d\nu\bar{\nu}$ [21]. Being usually ignored in the budget of theoretical uncertainties of Eq. (8), the importance of a complete calculation has recently been emphasized [22]. There, the NLO EW corrections in the limit of large top-quark mass have been employed, which is known to be insufficient at the level of accuracy aimed

at Ref. [21] and the residual EW uncertainties were estimated to be at least 5% on the branching ratio.

In Sec. II we describe the calculation of the NLO EW correction to $\mathcal{C}_{10}$ adopting the two choices of normalization and using different renormalization schemes for the involved EW parameters. In Sec. III, we summarize the solution of the RGE and obtain $\mathcal{C}_{10}$ at the low-energy scale of the order of the bottom-quark mass at the NLO in EW interactions. Finally, in Sec. IV we discuss the reduction of the EW renormalization-scheme dependences in $\mathcal{C}_{10}$ after the inclusion of NLO EW corrections. In the accompanying appendices A and B we collect additional technical information on the matching calculation and the RGE, respectively. Some supplementary details of Sec. IV have been relegated to App. C.

II. MATCHING CALCULATION OF NLO ELECTROWEAK CORRECTIONS

We obtain the EW NLO corrections to the Wilson coefficient $\mathcal{C}_{10}$ by matching the effective theory of EW interactions to the Standard Model. For this purpose we evaluate one-light-particle irreducible Greens functions with the relevant external light degrees of freedom up to the required order in the EW couplings in both theories. The Wilson coefficients are determined by requiring equality of the renormalized Greens functions order by order

$$\mathcal{A}_{\text{full}}(\mu_0) \overset{!}{=} \mathcal{A}_{\text{eff}}(\mu_0) \qquad (11)$$

at the matching scale μ_0. It is chosen of the order of the masses of the heavy degrees of freedom to minimize otherwise large logarithms that enter the Wilson coefficients. The Wilson coefficients have the general expansion

$$\begin{aligned} \mathcal{C}_i(\mu_0) = {} & \mathcal{C}_i^{(00)} + \tilde{\alpha}_s\,\mathcal{C}_i^{(10)} + \tilde{\alpha}_s^2\,\mathcal{C}_i^{(20)} \\ & + \tilde{\alpha}_e\left(\mathcal{C}_i^{(11)} + \tilde{\alpha}_s\,\mathcal{C}_i^{(21)} + \tilde{\alpha}_e\,\mathcal{C}_i^{(22)}\right) + \dots, \end{aligned} \qquad (12)$$

in the strong and electromagnetic $\tilde{\alpha}_{s,e} \equiv \alpha_{s,e}/(4\pi)$ running couplings of the effective theory at the scale μ_0, where we follow the convention of Ref. [23]. This expansion starts with tree-level contributions denoted by the superscript (00), has higher-order QCD corrections $(m0)$ with $m > 0$, pure QED corrections (mm) with $m > 0$ and mixed QCD-QED corrections (mn) with $m > n > 0$, all of which depend explicitly on μ_0 except for (00). For $\mathcal{C}_{10}$ the non-zero matching corrections start at order $\tilde{\alpha}_e$, i.e., for $n \geq 1$. The $\mathcal{C}_{10}^{(11)}$ [9] and $\mathcal{C}_{10}^{(21)}$ [17–20] contributions are known and here we calculate $\mathcal{C}_{10}^{(22)}$. Above, Eq. (12) has to be understood as the definition of the components $\mathcal{C}_i^{(mn)}$ that complies with the single-G_F normalization in the literature [23]. Comparison with Eqs. (6) and (7) yields

$$\mathcal{C}_{10}^{(11)} = \frac{4G_F}{\sqrt{2}} c_{10}^{(11)} = -\frac{4G_F}{\sqrt{2}} \frac{Y_0(x_t)}{s_W^2} \qquad (13)$$

and

$$\mathcal{C}_{10}^{(11)} = \frac{G_F^2 M_W^2}{\pi^2 \tilde{\alpha}_e} \tilde{c}_{10}^{(11)} = -\frac{G_F^2 M_W^2}{\pi^2 \tilde{\alpha}_e} Y_0(x_t) \qquad (14)$$

showing that this convention introduces an artificial factor $1/\alpha_e$ into the components in the case of the quadratic-G_F normalization. However, we will organize the renormalization group evolution (see Sec. III) such that these factors are of no consequence, as should be.

Although the operator P_{10} does not mix with other $\Delta B = 1$ operators under QCD, at higher order in QED interactions such a mixing does take place [23, 24]. As a consequence the effective Lagrangian (5) has to be extended

$$\mathcal{C}_{10} P_{10} \quad \longrightarrow \quad \sum_i \mathcal{C}_i P_i , \qquad (15)$$

where the term $\sim V_{ub} V_{uq}^* [\mathcal{C}_1 (P_1^c - P_1^u) + \mathcal{C}_2 (P_2^c - P_2^u)]$ does not contribute to the order considered here. The operators relevant to $B_q \to \ell^+ \ell^-$ at the considered order in strong and EW interactions comprise the current-current operators ($i = 1, 2$), QCD-penguin operators ($i = 3, 4, 5, 6$) and the semi-leptonic operator ($i = 9, 10$). We follow the operator definition of Ref. [23] that does not include the factor $\alpha_e/(4\pi)$ in $P_{9,10}$. This factor is included in the matching conditions of the Wilson coefficients at the matching scale μ_0 in Eq. (12). In the matching calculation only P_2 and P_9 as defined in App. A 1 are needed, whereas the remaining operators enter in the renormalization group evolution discussed in Sec. III.

We describe the calculation of $\mathcal{A}_{\text{full}}$ and $\mathcal{A}_{\text{eff}}$ in Sections II A and II B, respectively. In the SM calculation of $\mathcal{A}_{\text{full}}$, we apply different EW renormalization schemes for the involved parameters to demonstrate in Sec. IV that the renormalization scheme dependence is reduced to sub-percent effects when including $\mathcal{C}_{10}^{(22)}$. The schemes differ by finite parts of the counterterms that renormalize the bare parameters of the Lagrangian or equivalently the parameters appearing in the LO Wilson coefficient. Nevertheless, we use the same physical input in all schemes for the numerical evaluation that we have chosen to be

$$G_F, \quad \alpha_e(M_Z^{\text{pole}}), \quad \alpha_s(M_Z^{\text{pole}}),$$
$$V_{ij}, \quad M_Z^{\text{pole}}, \quad M_t^{\text{pole}}, \quad M_H^{\text{pole}} . \qquad (16)$$

G_F is the Fermi constant as extracted from muon lifetime experiments. It is itself a Wilson coefficient of the effective theory and plays thus a special role in the calculation of EW corrections; we postpone further discussion to Section II B. The couplings α_e and α_s are the $\overline{\text{MS}}$ couplings at the scale of the Z pole mass in the SM with decoupled top quark[2]. V_{ij} are elements of the CKM matrix. M_Z^{pole}, M_t^{pole} and M_H^{pole} are the pole masses of Z boson, top quark and Higgs boson, respectively. The numerical values are summarized in Tab. I.

---

[2] I.e. W and Z bosons are still dynamical degrees of freedom.

Parameter		Value	Ref.
G_F		$1.166\,379 \cdot 10^{-5}\,\text{GeV}^{-2}$	[11]
$\alpha_s(M_Z^{\text{pole}})$	$(N_f = 5)$	0.1184 ± 0.0007	[11]
$\alpha_e(M_Z^{\text{pole}})$	$(N_f = 5)$	$(127.944 \pm 0.014)^{-1}$	[11]
M_Z^{pole}		$(91.1876 \pm 0.0021)\,\text{GeV}$	[11]
M_t^{pole}		$(173.1 \pm 0.9)\,\text{GeV}$	[11, 25, 26]
M_H^{pole}		$(125.9 \pm 0.4)\,\text{GeV}$	[11, 27, 28]
$\Delta\alpha_{e,\text{hadr}}^{(5)}(M_Z^{\text{pole}})$		0.02772 ± 0.00010	[11]

TABLE I. The physical input. $\alpha_{s,e}$ are the running $\overline{\text{MS}}$ couplings of the five-flavor theory at $\mu = M_Z$. Masses are the experimentally measured pole masses.

A. Standard Model Calculation

We keep only the leading contributions of the expansion in the momenta of external states, in which case the full amplitude for $b \to q\ell^+\ell^-$ takes the form

$$\mathcal{A}_{\text{full}} = \sum_i A_{\text{full},i}(\mu) \langle P_i(\mu)\rangle^{(0)} . \qquad (17)$$

$\langle P_i(\mu)\rangle^{(0)}$ denote the tree-level matrix elements of operators mediating $b \to q\ell^+\ell^-$, i.e., $i = 9, 10$ as well as evanescent operators defined in App. A 1. The $A_{\text{full},i}$'s are coefficient functions with the electroweak expansion

$$A_{\text{full},i} = A_{\text{full},i}^{(0)} + \tilde{\alpha}_e A_{\text{full},i}^{(1)} + \tilde{\alpha}_e^2 A_{\text{full},i}^{(2)} + \dots , \qquad (18)$$

with α_e of the SM, i.e. six active quark flavors as well as heavy weak gauge bosons and the Higgs boson. In the case of the single-G_F normalization, $A_{\text{full},i}^{(0)} = 0$ for $b \to q\ell^+\ell^-$ mediating operators, whereas $A_{\text{full},i}^{(0)} \neq 0$ for the quadratic-G_F normalization due to the substitution $\alpha_e/s_W^2 \to G_F$.

Our focus here is the calculation of the two-loop contribution to $A_{\text{full},10}$ and some parts of $A_{\text{full},i}$ at one-loop that involve evanescent operators E_9 and E_{10} (see App. A 1). For this purpose, we calculate all two-loop EW Feynman diagrams and the corresponding one-loop diagrams with inserted counterterms, Fig. 1 depicts some examples. We proceed as in Ref. [21] and perform all calculations in the Feynman gauge $\xi = 1$ using two independent setups. Similarly to Ref. [21] also here we find contributions from electroweak gauge bosons that are $1/s_W^2$ enhanced. In App. A 2 we discuss the more technical aspects of the calculation, e.g. γ-algebra in d-dimensions and loop-integrals. Here, we concentrate on the electroweak renormalization conditions.

Having fixed the physical input, we define three renormalization schemes and discuss the relation of their renormalized parameters to the physical input in Eq. (16). In all three schemes we use $\overline{\text{MS}}$ renormalization for α_e and the top-quark mass under QCD, whereas additional finite terms are included into the field renormalization constants as explained in more detail in
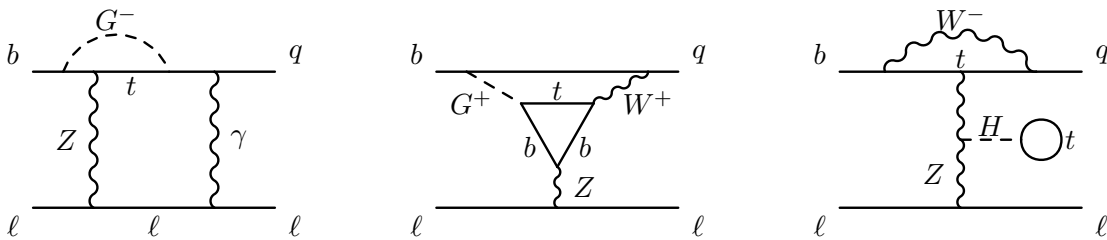
FIG. 1. Two-loop diagrams in the SM contributing to the $b \to q\ell^+\ell^-$ at NLO in EW interactions.

App. A 2. Therefore, our schemes differ only by finite EW renormalizations of s_W, M_t and M_W appearing at LO in c_{10}. For $\widetilde{c}_{10}$, s_W is absorbed in the additional factor G_F and needs no further specification.

1.) On-shell scheme

In the on-shell scheme, at the order we consider, the on-shell masses of Z boson and top quark coincide with their pole masses. The mass of the W boson is a dependent quantity for our choice of physical input. We calculate it including radiative corrections following Ref. [29]. This relation introduces a mild Higgs-mass dependence of $\mathcal{C}_{10}$ at LO. The weak mixing angle in the on-shell scheme is defined by

$$s_W^2 \equiv (s_W^{\text{on-shell}})^2 = 1 - \left(M_W^{\text{on-shell}}/M_Z^{\text{on-shell}}\right)^2 . \quad (19)$$

Therefore, the only finite counterterms necessary are δM_Z^2, δM_W^2 and δM_t at one-loop, they are given in Refs. [30, 31]. We also treat tadpoles as in Refs. [30, 31]: we include tadpole diagrams (see Fig. 1), and a renormalization δt to cancel the divergence and the finite part of the one-loop tadpole diagram. This way we ensure that all renormalization constants apart from wave function renormalizations are gauge invariant [32].

2.) $\overline{\text{MS}}$ scheme

In the $\overline{\text{MS}}$ scheme the fundamental parameters are those of the "unbroken" SM Lagrangian

$$g_1, \qquad g_2, \qquad g_3, \qquad v, \qquad \lambda \quad \text{and} \quad y_t. \quad (20)$$

Here g_3, g_2 and g_1 are the couplings of the SM gauge group $SU(3)_c \times SU(2)_L \times U(1)_Y$, v is the vacuum expectation value of the Higgs field and λ its quartic self-coupling, whereas y_t is the top-Yukawa coupling. The parameters are renormalized by counterterms subtracting only divergences and $\log(4\pi) - \gamma_E$ terms, i.e., they are running $\overline{\text{MS}}$ parameters. We do not treat tadpoles differently in this respect, only their divergences are subtracted by the counterterm for v. By expressing the parameters of the LO Wilson coefficients in terms of the "unbroken"-phase parameters

$$s_W^2 = g_1^2/(g_1^2 + g_2^2), \quad 4\pi\alpha_e = g_1^2 g_2^2/(g_1^2 + g_2^2),$$
$$M_W = vg_2/2, \qquad\qquad x_t = 2y_t^2/g_2^2, \quad (21)$$

we iteratively fix the values of the "unbroken" parameters at the matching scale μ_0. To this end, we require

that the physical input in Eq. (16) is reproduced to one-loop accuracy.

3.) Hybrid scheme

For Eq. (7), where s_W appears at LO, we may adopt yet another scheme. We renormalize the couplings α_e and s_W in the $\overline{\text{MS}}$ scheme and the masses in x_t on-shell. Effectively this corresponds to including the on-shell counterterms for masses and using Eq. (21) instead of Eq. (19) for s_W. Correspondingly, we use s_W, α_e, M_t, M_W and M_H as fundamental parameters for the hybrid scheme. This scheme is a better-behaved alternative to the on-shell scheme, in which the counterterm for s_W receives large top-quark mass dependent corrections. (see App. C).

Having fixed all renormalization conditions we evaluate $A_{\text{full},10}^{(2)}$. In practice we calculate the $\overline{\text{MS}}$ amplitude and include the appropriate counterterms in $A_{\text{full},10}^{(1)}$ to shift from the $\overline{\text{MS}}$ to the on-shell or hybrid scheme. The full expression for $A_{\text{full},10}^{(2)}$ is too lengthy to be included here[3].

B. Effective Theory Calculation

The effective theory is described by the effective Lagrangian in Eqs. (5) and (15) with canonically normalized kinetic terms for all fields. To simplify the notation we drop any indices indicating an expansion in $\tilde{\alpha}_s$ throughout this Section. The fields and couplings are $\overline{\text{MS}}$-renormalized via the redefinitions of bare quantities

$$d \to \sqrt{Z_d}\,d\,, \quad \ell \to \sqrt{Z_\ell}\,\ell\,, \quad C_j \to \sum_i C_i \hat{Z}_{i,j}\,, \quad (22)$$

where d denotes down-type quark fields and ℓ denotes charged-lepton fields. The renormalization constant of the Wilson coefficients is the matrix $\hat{Z}_{i,j}$ arising from operator mixing. It has an expansion in $\tilde{\alpha}_e$

$$\hat{Z}_{i,j} = \delta_{i,j} + \tilde{\alpha}_e\,\hat{Z}_{i,j}^{(1)} + \tilde{\alpha}_e^2\,\hat{Z}_{i,j}^{(2)} + \dots \quad (23)$$

----

[3] We attach the complete analytic two-loop EW contribution in the on-shell scheme for the quadratic-G_F normalization, $\widetilde{c}_{10}^{(22)}$, to the electronic preprint.

analogously to the expansion of the renormalization constants of the fields and couplings given in Eq. (A12).

All loop diagrams in the effective theory vanish, since we set all light masses to zero, expand in external momenta and employ dimensional regularization. Accordingly, the effective theory amplitude is entirely determined through the product of tree-level matrix elements $\langle P_j \rangle^{(0)}$, the Wilson coefficients $\mathcal{C}_i$ and appropriate renormalization constants. The renormalized amplitude reads

$$
\begin{aligned}
\mathcal{A}_{\text{eff}}(\mu) &= \sum_i A_{\text{eff},\,i}(\mu) \langle P_i(\mu) \rangle^{(0)} \\
&= V_{tb} V_{tq}^* \sum_{i,j} \mathcal{C}_i(\mu)\, \hat{Z}_{i,j} Z_j \, \langle P_j(\mu) \rangle^{(0)} .
\end{aligned}
\tag{24}
$$

As mentioned above, both the Wilson coefficients $\mathcal{C}_i$ and the renormalization constants are expanded in $\tilde{\alpha}_e$ as given in Eqs. (12) and (23), respectively. The Z_j's summarize products of field- and charge-renormalization constants of the operator in question, i.e. for P_{10}

$$
Z_{10} = Z_d Z_\ell ,
\tag{25}
$$

which is the one required up to two-loop level in $\tilde{\alpha}_e$.

Only a few physical operators contribute to the part of the amplitude in Eq. (24) proportional to $\langle P_{10} \rangle^{(0)}$ since only a few mix either at one-loop or two-loop level into P_{10} and have, at the same time, a non-zero Wilson coefficient at one-loop or tree-level, respectively. These are: the operator P_2 having a non-zero Wilson coefficient $\mathcal{C}_2^{(00)}$ as well as an entry in $\hat{Z}_{2,10}^{(2)}$ and P_9 that mixes at one-loop into P_{10} and have a non-vanishing $\mathcal{C}_i^{(11)}$. Apart from the physical operators also one evanescent operator, i.e. E_9 contributes. We give the definition of the operators in App. A 1 and present some details on the calculation of the renormalization constants in the five-flavor theory in App. A 3. All contributing mixing renormalization constants of physical operators can be extracted from the anomalous dimension in the literature [24]. We collect all constants and discuss the mixing of evanescent operators in App. A 3. Finally, at the two-loop level

$$
\begin{aligned}
A_{\text{eff},10}^{(2)} = V_{tb} V_{tq}^* (\tilde{\alpha}_e)^n \bigg[&\mathcal{C}_{10}^{(22)} + \mathcal{C}_{10}^{(11)} Z_{10}^{(1)} \\
&+ \mathcal{C}_2^{(00)} \hat{Z}_{2,10}^{(2)} + \sum_{i=9,E_9} \mathcal{C}_i^{(11)} \hat{Z}_{i,10}^{(1)} \bigg]
\end{aligned}
\tag{26}
$$

with the power $n = 2$ and $n = 1$ for the single- and quadratic-G_F normalization, respectively. In this equation α_e is the electromagnetic coupling constant in the $\Delta B = 1$ effective theory. It differs from the one in Tab. I by threshold corrections due to W and Z gauge bosons and from the one in the SM in Eq. (18) by the additional top-quark threshold corrections as explained above Eq. (A9). Note that the renormalization constant $\hat{Z}_{2,10}^{(2)}$, see Eq. (A14), implies the existence of a quadratic logarithm that will be resummed with the help of the RGE in Sec. III.

The one-loop Wilson coefficients in Eq. (26), multiplied with renormalization constants, contribute finite terms to the matching through their $\mathcal{O}(\epsilon)$ terms. We reproduce the finite and $\mathcal{O}(\epsilon)$ parts of $\mathcal{C}_{9,10}^{(11)}$ in [33]. For $\mathcal{C}_{E_9}^{(11)}$ only the finite term is needed, we give it in App. A 3. For this purpose we have matched also the one-loop amplitudes proportional to the $\langle P_{9,10}, E_9 \rangle^{(0)}$ keeping $\mathcal{O}(\epsilon)$ terms when required.

The Fermi constant, G_F, is very precisely measured in muon decay and provides a valuable input for the determination of the EW parameters. Following [21], we define G_F to be proportional to the Wilson coefficient G_μ of the operator $Q_\mu = (\bar{\nu}_{\mu_L} \gamma_\rho \mu_L)(\bar{e}_L \gamma^\rho \nu_{e_L})$ that induces muon decay in the effective Fermi theory

$$
G_F \equiv \frac{1}{2\sqrt{2}} G_\mu = \frac{1}{2\sqrt{2}} \left(G_\mu^{(0)} + \tilde{\alpha}_e G_\mu^{(1)} + \dots \right) ,
\tag{27}
$$

with the tree-level matching relation

$$
G_\mu^{(0)} = \frac{2\pi\alpha_e}{s_W^2 M_W^2} = \frac{2}{v^2}
\tag{28}
$$

and the NLO EW correction $G_\mu^{(1)}$. Since we work at NLO in EW interactions, $G_\mu^{(1)}$ enters the effective theory amplitude in Eq. (24). Moreover, the power of G_F in the normalization of the effective Lagrangian affects the matching contribution of $G_\mu^{(1)}/G_\mu^{(0)} \times \mathcal{C}_i^{(11)}$ to $\mathcal{C}_i^{(22)}$, in contrast to the leading EW components $\mathcal{C}_i^{(11)}$ that remain unchanged when using different powers. This can be best understood by the explicit $\tilde{\alpha}_e$ expansion for the single-G_F normalization

$$
\mathcal{C}_{10} \sim G_F \, c_{10} \sim \left[G_\mu^{(0)} + \tilde{\alpha}_e G_\mu^{(1)} \right] \left[c_{10}^{(11)} + \tilde{\alpha}_e \, c_{10}^{(22)} \right]
\tag{29}
$$

$$
= G_\mu^{(0)} \left[c_{10}^{(11)} + \tilde{\alpha}_e \left(c_{10}^{(22)} + \frac{G_\mu^{(1)}}{G_\mu^{(0)}} c_{10}^{(11)} \right) \right] + \mathcal{O}(\tilde{\alpha}_e^2)
$$

and the quadratic-G_F normalization

$$
\mathcal{C}_{10} \sim (G_\mu^{(0)})^2 \left[\tilde{c}_{10}^{(11)} + \tilde{\alpha}_e \left(\tilde{c}_{10}^{(22)} + 2 \frac{G_\mu^{(1)}}{G_\mu^{(0)}} \tilde{c}_{10}^{(11)} \right) \right] ,
\tag{30}
$$

which receives an additional factor of 2. Depending on the choice of normalization, the according contribution proportional to $G_\mu^{(1)}/G_\mu^{(0)} \times \mathcal{C}_i^{(11)}$ enters Eq. (26).

The merit of defining G_F to be itself a Wilson coefficient at the matching scale is that the large uncertainties from the scale dependence of the vacuum expectation value in $G_\mu^{(0)}$ do not appear at all at LO in the Wilson coefficient.

This way, we obtain $\mathcal{C}_{10}^{(22)}$, which has been known only in the large top-quark-mass limit [34, 35], by matching the parts of $A_{\text{eff}} \sim \langle P_{10} \rangle^{(0)}$ and $A_{\text{full}} \sim \langle P_{10} \rangle^{(0)}$ at NLO order in $\tilde{\alpha}_e$ and verify the explicit cancellations of all left-over divergences.

III. RENORMALIZATION GROUP EVOLUTION

This section summarizes the results of the evolution of the Wilson coefficients under the renormalization group equations from the matching scale μ_0 down to the low scale μ_b. The matching scale μ_0 is of the order of the masses of the decoupled heavy degrees of freedom ~ 100 GeV and $\mu_b \sim 5$ GeV of the order of the bottom-quark mass at which matrix elements are evaluated. The according anomalous dimension matrices of the $\Delta B = 1$ effective theory, including NLO EW corrections, are given in Ref. [24] and the RGE is solved in Ref. [23] for the single-G_F normalized Lagrangian in Eqs. (5) and (7) including the running of α_e. These corrections have already been considered in Ref. [10] in the analysis of $B_q \to \ell^+\ell^-$.

The evolution operator $U(\mu_b, \mu_0)$ relates the Wilson coefficients at the matching scale, see Eq. (12), to the ones at μ_b:

$$\mathcal{C}_i(\mu_b) = \sum_j U(\mu_b, \mu_0)_{ij}\, \mathcal{C}_j(\mu_0)\,. \tag{31}$$

At the low-energy scale the Wilson coefficients may again be expanded in $\alpha_s(\mu_b)$ and the small ratio $\kappa \equiv \alpha_e(\mu_b)/\alpha_s(\mu_b)$:

$$\mathcal{C}_i(\mu_b) = \sum_{m,n=0} [\tilde{\alpha}_s(\mu_b)]^m\, [\kappa(\mu_b)]^n\, \mathcal{C}_{i,(mn)}\,. \tag{32}$$

We obtain the explicit expressions for the components $\mathcal{C}_{i,(mn)}(\mu_b)$ from the solution given in Ref. [23] with further details and the solution for $i = 10$ presented in App. B.

In the single-G_F normalization the Wilson coefficient $c_{10}(\mu_b)$ starts at order α_e with the following non-zero contributions

$$c_{10}(\mu_b) = \tilde{\alpha}_e \left(c_{10,(11)} + \tilde{\alpha}_s c_{10,(21)} \right)$$
$$+ \tilde{\alpha}_e^2 \left(\frac{c_{10,(02)}}{\tilde{\alpha}_s^2} + \frac{c_{10,(12)}}{\tilde{\alpha}_s} + c_{10,(22)} \right)\,. \tag{33}$$

The components $c_{i,(mn)}$ are functions of the ratio $\eta \equiv \alpha_s(\mu_0)/\alpha_s(\mu_b)$ and the high-scale components $c_j^{(mn)}$ of Eq. (12). For illustration, we give here numerical results for the exemplary values $\mu_0 = 160$ GeV and $\mu_b = 5$ GeV,

yielding $\eta = 0.509$,

$$c_{10,(11)} = c_{10}^{(11)}\,,$$

$$c_{10,(21)} = \eta\, c_{10}^{(21)}\,,$$

$$c_{10,(02)} = 0.0058\, c_2^{(00)}\,,$$

$$c_{10,(12)} = 0.068\, c_2^{(00)} + 0.005\, c_1^{(10)} - 0.005\, c_4^{(10)}$$
$$+ 0.252\, c_9^{(11)} + 1.118\, c_{10}^{(11)}\,, \tag{34}$$

$$c_{10,(22)} = 0.133\, c_1^{(10)} + 0.066\, c_4^{(10)}$$
$$+ 0.002\, c_1^{(20)} + 0.001\, c_2^{(20)} + 0.004\, c_3^{(20)}$$
$$- 0.002\, c_4^{(20)} + 0.033\, c_5^{(20)} - 0.039\, c_6^{(20)}$$
$$- 1.593\, c_9^{(11)} - 2.226\, c_{10}^{(11)}$$
$$+ 0.128\, c_9^{(21)} + 0.569\, c_{10}^{(21)} + c_{10}^{(22)}\,.$$

We give the explicit solution for arbitrary values of η in App. B 2. Furthermore, the $c_{10,(mn)}$ depend on the initial matching conditions of the Wilson coefficients, the $c_i^{(mn)}$ in Eq. (12), at various orders: tree-level for $i = 2$, one-loop in α_s for $i = 1, 4$ and in α_e for $9, 10$ and two-loop in α_s^2 for $i = 1, \ldots, 6$ and in $\alpha_e\alpha_s$ for $i = 9, 10$ [33] as well as the two-loop NLO EW correction for $i = 10$ presented in Sec. II.

We derive the equivalent expressions for the case of the quadratic-G_F normalization from the single-G_F normalization in Eq. (32)

$$\tilde{c}_i(\mu_b) = \sum_{m,n=0} [\tilde{\alpha}_s(\mu_b)]^{m-1}\, [\kappa(\mu_b)]^{n-1}\, \tilde{c}_{i,(mn)}\,. \tag{35}$$

For $i = 10$ the lowest-order non-zero terms

$$\tilde{c}_{10}(\mu_b) = \tilde{c}_{10,(11)} + \tilde{\alpha}_s \tilde{c}_{10,(21)}$$
$$+ \tilde{\alpha}_e \left(\frac{\tilde{c}_{10,(02)}}{\tilde{\alpha}_s^2} + \frac{\tilde{c}_{10,(12)}}{\tilde{\alpha}_s} + \tilde{c}_{10,(22)} \right)\,, \tag{36}$$

already start at order α_e^0. The components of the initial Wilson coefficients in Eq. (12) are related as

$$\tilde{c}_i^{(mn)} = s_W^2\, c_i^{(mn)} \qquad \text{for} \quad n < 2\,, \tag{37}$$

where a factor $\tilde{\alpha}_e(\mu_0)$ has been pulled out and substituted by $\tilde{\alpha}_e(\mu_b)$. For cases $n \geq 2$, which is here only of concern for $\mathcal{C}_{10}$, an additional shift has to be taken into account explicitly in the matching analogously to the discussion below Eq. (27). Eventually, the downscaled components $\tilde{c}_{i,(mn)}$ in Eq. (35) are given by Eq. (34) with the replacement $c_i^{(mn)} \to \tilde{c}_i^{(mn)}$ and by omitting the contributions of $\tilde{c}_{10}^{(11)}$ in $\tilde{c}_{10,(12)}$ as well as $\tilde{c}_{10}^{(11)}$ and $\tilde{c}_{10}^{(21)}$ in $\tilde{c}_{10,(22)}$, as explained in more detail in App. B.

IV. NUMERICAL IMPACT OF NLO EW CORRECTIONS

In Sec. II we presented the details of the calculation of the complete NLO EW matching corrections to the Wilson coefficient $\mathcal{C}_{10}$ in the SM and in Sec. III the effects of the renormalization group evolution within the $\Delta B = 1$ effective theory from the matching scale μ_0 to the low energy scale μ_b. In this section, we discuss the numerical impact of these corrections on $\mathcal{C}_{10}$ at both scales and assess the reduction of theoretical uncertainties associated with the different choices of the renormalization scheme. Finally, we shall briefly comment on the branching ratio $\mathrm{Br} \propto |\mathcal{C}_{10}|^2$.

Throughout, we use the four-loop β function for α_s including the three-loop mixed QCD×QED term given in Ref. [23]. When crossing the $N_f = 5$ to $N_f = 6$ threshold at the matching scale μ_0, we include the three-loop QCD threshold corrections using the pole-mass value for the top-quark mass M_t^{pole} (see Tab. I). The running of α_e is implemented including the two-loop QED and three-loop mixed QED×QCD terms presented in [23], where the threshold corrections have been omitted when crossing the $N_f = 5$ to $N_f = 6$ threshold entering the evolution of α_s. We list the initial conditions for the coupling constants in Tab. I and remark that the value of α_e given in Ref. [11] refers to the coupling within the SM with the top quark decoupled. From this value we determine α_e at $\mu = M_Z$ in the SM with $N_f = 6$ with the help of the decoupling relation of Eq. (A9) thereby omitting the constant and logarithmic term from the gauge boson contribution and determine the dependent EW parameters as described in Sec. II A. The value of α_e in the effective theory is found as described below the decoupling relation of Eq. (A9).

We determine the running top-quark mass in the $\overline{\mathrm{MS}}$ scheme with respect to QCD from M_t^{pole} with the aid of the three-loop relation[4], $m_t(m_t) = 163.5$ GeV, and evolve it to the matching scale applying the four-loop expression of the quark-mass anomalous dimension. Here m_t denotes the top-quark mass, where QCD corrections are $\overline{\mathrm{MS}}$-renormalized, but EW corrections are considered in the on-shell scheme. In the case that the latter are also $\overline{\mathrm{MS}}$-renormalized, we shall choose the notation $\overline{m}_t$. The additional shift from $m_t \to \overline{m}_t$, while numerically quite significant yielding $\overline{m}_t(\overline{m}_t) = 172.4$ GeV, is dominated by the contribution of tadpole diagrams. The tadpole-induced shift cancels in the ratio $x_t = \overline{m}_t^2 / \overline{M}_W^2$ entering the LO Wilson coefficient.

As already emphasized in Sec. II, once considering higher EW corrections, the different choices of normalization of the effective Lagrangian from Eq. (6) affects

---

[4] The choice of the matching scale that determines the $N_f = 5$ to $N_f = 6$ threshold has a numerically negligible impact for $\mu_0 \in [50, 300]$ GeV considered here.

differently the NLO EW matching corrections of $\mathcal{C}_{10}$. As renormalization schemes (RS) we consider the on-shell scheme, the $\overline{\mathrm{MS}}$ scheme and the hybrid scheme introduced in Sec. II A, which we abbreviate in the following as RS = OS, $\overline{\mathrm{MS}}$ and HY. We apply both, the single-G_F and the quadratic-G_F normalization for the on-shell scheme denoted as RS = OS-1 and OS-2, respectively. For RS = $\overline{\mathrm{MS}}$ and HY we use only the single-G_F normalization.

We first consider the size and the reduction of the scheme dependences in $\mathcal{C}_{10}$ at the matching scale

$$
\mathcal{C}_{10}(\mu_0) = \begin{cases} \dfrac{4G_F}{\sqrt{2}} \tilde{\alpha}_e(\mu_0) \left[c_{10}^{(11)} + \tilde{\alpha}_e(\mu_0)\, c_{10}^{(22)}(\mu_0) \right] \\[2ex] \dfrac{G_F^2 M_W^2}{\pi^2} \left[\widetilde{c}_{10}^{(11)} + \tilde{\alpha}_e(\mu_0)\, \widetilde{c}_{10}^{(22)}(\mu_0) \right] \end{cases},
$$

$$(38)$$

for the single- and quadratic-G_F normalization respectively, after including the NLO EW corrections $\mathcal{C}_{10}^{(22)}$. To separate the effects of the EW calculation, we first switch off any QCD dependence. Namely, we omit the NLO QCD correction $\mathcal{C}_{10}^{(21)}$ and neglect the μ_0 dependence of the top-quark mass under QCD by fixing the QCD scale and using $m_t(m_t)$ as the on-shell top-quark mass under EW renormalization, as far as OS-1, OS-2 and HY schemes are concerned. In the $\overline{\mathrm{MS}}$ scheme we perform the additional shift $m_t \to \overline{m}_t$ using the value of $m_t(m_t)$ as input value. Note, that for the choice of scale of m_t in the running QCD top mass, the omitted NLO QCD correction $\mathcal{C}_{10}^{(21)}$ is particularly small [18–20], i.e. the LO result $\mathcal{C}_{10}^{(11)}$ accounts for the dominant part of the higher-order QCD correction.

The LO and (LO + NLO EW) results are depicted in Fig. 2 for the four renormalization schemes. For μ_0-independent top-quark mass the LO $\mathcal{C}_{10}$ is μ_0 independent in the OS-2 scheme, whereas the replacement $G_F \to \alpha_e(\mu_0)/(s_W^{\mathrm{on-shell}})^2$ introduces a μ_0 dependence in OS-1 and a quite significant shift of about 4% with respect to OS-2, which translates into a 8% change of the LO branching ratio. Although based on the same single-G_F normalization, the $\overline{\mathrm{MS}}$ and HY schemes exhibit relatively large shifts with respect to OS-1 and a modified μ_0 dependence due to the $\overline{\mathrm{MS}}$ renormalization of s_W in both, HY and $\overline{\mathrm{MS}}$, schemes and additionally the EW $\overline{\mathrm{MS}}$ renormalization of the top-quark and W mass in the $\overline{\mathrm{MS}}$ scheme. The overall uncertainty due to EW corrections at LO may be estimated from the variation of $\mathcal{C}_{10}$ given by all four schemes ranging in the interval $\mathcal{C}_{10}(\mu_0) \in [-8.9, -8.2] \cdot 10^{-8}$ for $\mu_0 \in [50, 300]$ GeV corresponding to a ±8% uncertainty on the level of the branching ratio. The inclusion of the NLO EW corrections eliminates this large uncertainty, as all four schemes yield aligned (LO + NLO EW) results and the μ_0 dependence cancels to large extent in all schemes. The residual uncertainty due to EW corrections is now confined to the small interval of $\mathcal{C}_{10}(\mu_0) \in [-8.31, -8.25] \cdot 10^{-8}$ at the
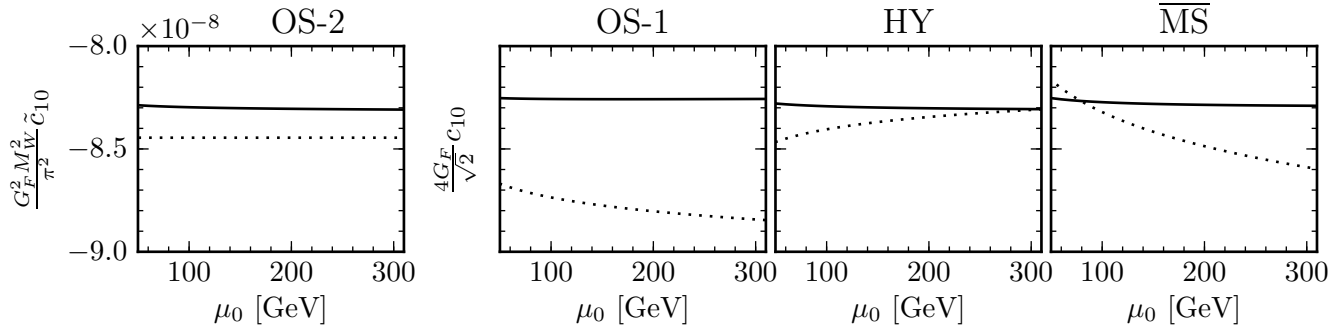
FIG. 2. Comparison of the matching scale, μ_0, dependence of $\mathcal{C}_{10}$ at the scale μ_0 in four renormalization schemes (OS-2, OS-1, HY and $\overline{\text{MS}}$) at LO (dotted) and with NLO EW corrections (solid). See text for more details.

scale μ_0, it is less than $\pm 0.4\%$ corresponding to $\pm 0.8\%$ on the branching ratio. The strong reduction of the μ_0 dependence in Fig. 2 is due to the inclusion of NLO corrections in the relation of EW parameters, which are formally not part of the effective theory and hence cannot be cancelled by the RGE in the effective theory. At LO in the effective theory there is no renormalization group mixing of $\mathcal{C}_{10}$ and the μ_0 dependence may be used directly as an uncertainty. As discussed in Sec. III, beyond LO in QED the operator mixing will reduce the remaining μ_0 dependence even further.

Before proceeding, we comment on the OS-1 and $\overline{\text{MS}}$ scheme and why we shall discard them for the estimate of residual higher-order uncertainties. The OS-1 scheme exhibits the worst perturbative behavior of all four schemes, as seen in Fig. 2. The s_W-on-shell counterterm induces this, for an electroweak correction, unnaturally large shift at two-loop. As further discussed in App. C, the top-quark mass dependence of the s_W-on-shell counterterm implies a significant higher-order QCD scale dependence, which we consider artificial. On the other hand, the OS-2 and HY schemes do not exhibit this strong dependence on the top-quark mass and the estimate of the size of higher-order QCD contributions by varying the scale of m_t indicates much smaller corrections. In view of this, we restrict ourselves to schemes with reasonable convergence properties and leave OS-1 aside. In the case of the $\overline{\text{MS}}$ scheme, the application of RG equations is required for the iterative determination of the EW parameters from the input given in Eq. (16). For the purpose of Fig. 2, the presence of QCD could be ignored and lowest-order RG equations were sufficient. However, in the general case the solution of the according RG equations are rather involved and we prefer to use the comparison of the HY and OS-2 scheme to estimate higher order EW×QCD corrections.

In the following, we include QCD effects and discuss $\mathcal{C}_{10}$ at the low-energy scale μ_b after applying the RGE running presented in Sec. III. We express the Wilson coefficient $\mathcal{C}_{10}(\mu_b)$ as a double series in the running couplings $\tilde{\alpha}_s$ and $\tilde{\alpha}_e$, see Eqs. (32) and (34), with five relevant contributions $\mathcal{C}_{10,(mn)}$, $(mn = 11, 21, 02, 12, 22)$, that depend on Wilson coefficients of various other operators at the matching scale μ_0. So far, only the LO $\equiv (mn = 11)$ and the NLO QCD $\equiv (mn = 11 + 21)$ contributions were known. Now, we can include the full NLO EW correction with the additional contributions $(mn = 11 + 21 + 02 + 12 + 22) \equiv$ NLO $(\text{QCD} + \text{EW})$[5]. For this purpose, also the scale dependence of m_t that originates from QCD will be taken into account when varying the matching scale μ_0. Note that $\mathcal{C}_{10}(\mu_b)$ is independent of the matching scale μ_0 up to the considered orders in couplings due to the inclusion of the RGE evolution. However, the residual μ_b dependence will only be cancelled by the according μ_b dependence of the matrix elements of the relevant operators.

Fig. 3 shows the μ_0 dependence of $\mathcal{C}_{10}(\mu_b = 5\,\text{GeV})$ at LO, NLO QCD and NLO $(\text{QCD} + \text{EW})$ in the OS-2 and HY schemes. It is clearly visible that the dependence on the renormalization scale of m_t reduces when going from LO to NLO QCD and that the LO results coincide with the ones at NLO QCD at the scale $\mu_0 \approx 150$ GeV. A further reduction of this scheme dependence requires the inclusion of NNLO QCD corrections [36]. The NLO QCD result is quite different in the OS-2 and HY scheme comprising values of $\mathcal{C}_{10}(\mu_b) \in [-8.54, -7.97] \cdot 10^{-8}$. The NLO $(\text{QCD} + \text{EW})$ result shows again rather large shifts with respect to NLO QCD and a clear convergence of both schemes towards the same value. The results of the OS-2 and HY schemes are now confined within $\mathcal{C}_{10}(\mu_b) \in [-8.34, -8.11] \cdot 10^{-8}$ reducing the combined uncertainty due to scheme dependencies of both QCD and EW interactions to $\pm 1.4\%$. Again, we would like to remind that a substantial part of this uncertainty is due to so far unknown NNLO QCD corrections. We estimate

_____

[5] These corrections were discussed in the large top-quark-mass limit including the RGE effects in Ref. [10], whereas RGE effects were neglected in Ref. [22] for $(mn = 02, 12, 22)$.
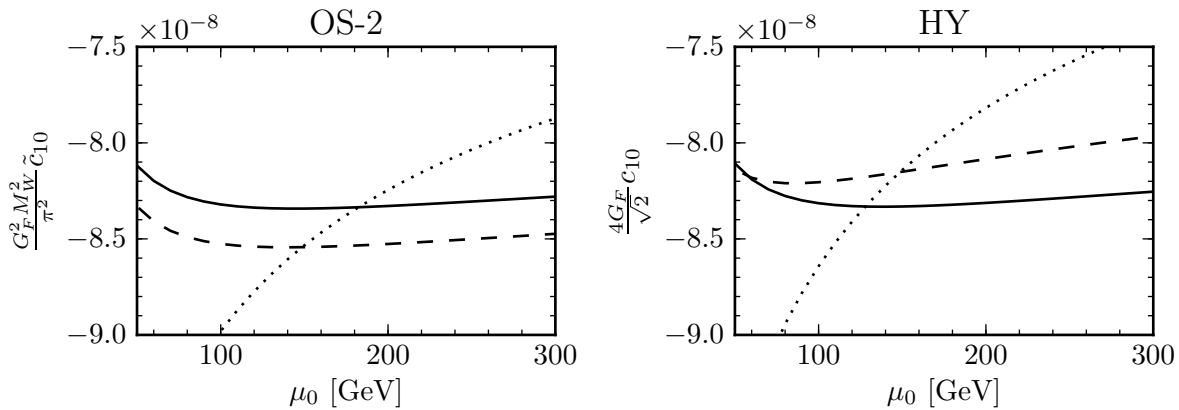
FIG. 3. The μ_0 dependence of the Wilson coefficient $\mathcal{C}_{10}(\mu_b = 5\,\text{GeV})$ in two renormalization schemes (OS-2, HY) at LO (dotted), NLO QCD (dashed) and NLO (QCD + EW) (solid). See text for more details.
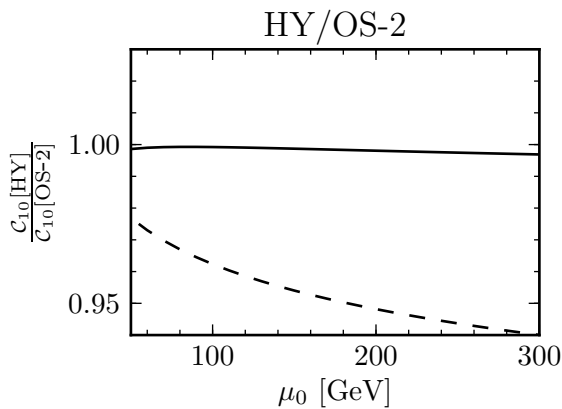

FIG. 4. The μ_0 dependence of the ratio of the Wilson coefficient $\mathcal{C}_{10}(\mu_b = 5\,\text{GeV})$ in the HY and the OS-2 scheme at LO and NLO QCD (dashed) and NLO (QCD + EW) (solid). LO and NLO QCD curves coincide.

the uncertainty due to higher-order EW and QCD corrections to our two-loop EW result from 1) the ratio of the results of the HY to the OS-2 scheme, thereby eliminating the numerically leading QCD μ_0-dependence of m_t, and 2) by varying the scale μ_0 only in m_t of the two-loop EW matching corrections $c_{10}^{(22)}$ (or $\tilde{c}_{10}^{(22)}$). As can be seen in Fig. 4, at the level of NLO QCD the ratio deviates quite strongly from 1 whereas at NLO (QCD + EW) the deviations are less than 0.3%. The ratio of the LO results coincides with the ratio of the NLO QCD one. We find a similar μ_0 dependence of the OS-2 and HY results (about $\pm0.1\%$) when varying the scale only in m_t of the EW two-loop matching correction. We choose the OS-2 scheme with $\mu_0 = 160$ GeV to predict the central value of $\mathcal{C}_{10} = -8.341 \cdot 10^{-8}$, the HY scheme

yields $-8.329 \cdot 10^{-8}$, and we assign an error due to higher-order EW corrections from the variation of μ_0 of about $\pm0.3\%$ as suggested by the comparison of the OS-2 and HY schemes.

We now turn to the discussion of the residual μ_b dependence for the fixed value $\mu_0 = 160$ GeV. As already mentioned above, including the according matrix elements of the involved operators shall decrease this dependence further, however, for the moment it remains an additional source of uncertainty. Fig. 5 shows $\mathcal{C}_{10}(\mu_b)$ at LO, NLO QCD and NLO (QCD + EW) in the OS-2 and HY schemes. Whereas the values of $\mathcal{C}_{10}(\mu_b)$ are quite different in all three schemes at NLO QCD, the inclusion of NLO (QCD + EW) corrections in the form of the renormalization group evolution yields a convergence towards the same value and a very small residual μ_b dependence in each scheme of less than $\pm0.2\%$ (OS-2: $\pm0.16\%$ and HY: $\pm0.20\%$) when varying $\mu_b \in [2.5, 10]$ GeV. We would like to note, that the non-perturbative uncertainty due to unknown QED corrections in the evaluation of the matrix elements is an additional source of uncertainty, not included in the above estimate.

The dependence of the EW corrections on the Higgs mass is entirely negligible. Varying $M_H \in [120, 130]$ GeV induces variations in $\mathcal{C}_{10}$ of less than $\pm0.01\%$.

As our final result we choose for the central value the OS-2 scheme with scale settings $\mu_0 = 160$ GeV and $\mu_b = 5$ GeV

$$\mathcal{C}_{10} = (-8.34 \pm 0.04) \cdot 10^{-8}, \qquad (39)$$

where we have estimated higher-order corrections of EW origin from the scale variations of $\mu_0 \in [50, 300]$ GeV and $\mu_b \in [2.5, 10]$ GeV in two schemes, OS-2 and HY, and added linearly the two errors. We have not included into the error budget the residual errors associated to higher QCD corrections that can be removed by means of the NNLO QCD calculation [36] nor any of the parametric
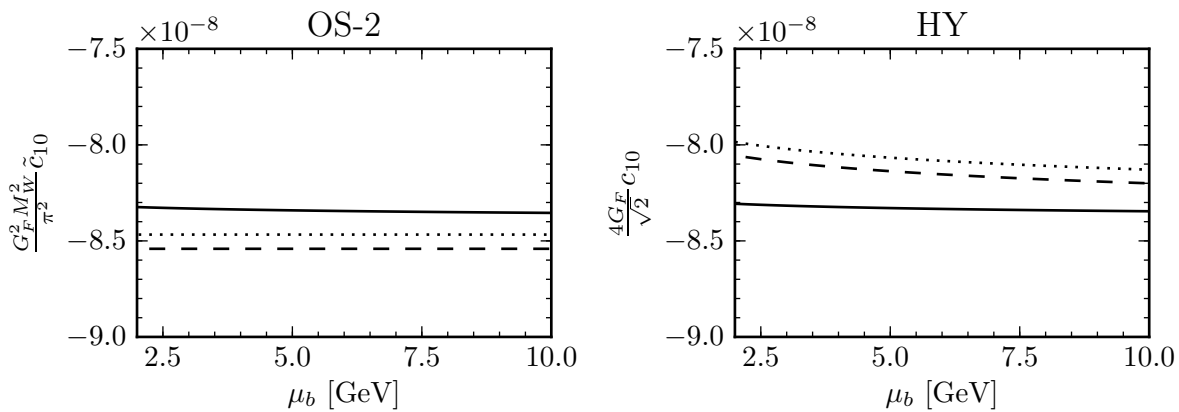
FIG. 5. The μ_b dependence of the Wilson coefficient $\mathcal{C}_{10}(\mu_b)$ for fixed $\mu_0 = 160$ GeV in two renormalization schemes (OS-2, HY) at LO (dotted), NLO QCD (dashed) and NLO (QCD + EW) (solid). See text for more details.

errors listed in Tab. I. To show the improvements of our final result (39), we quote for comparison the results at NLO QCD

$$\mathcal{C}_{10}^{\text{OS-2}} = -8.54 \cdot 10^{-8}, \quad \mathcal{C}_{10}^{\text{HY}} = -8.14 \cdot 10^{-8} \quad (40)$$

taken from the according curves of the OS-2 and HY schemes in Fig. 3.

Finally, we compare our prediction with the previous estimate [22], which was obtained using the large-m_t approximation of $\mathcal{C}_{10}^{(22)}$ and neglecting the effects of the RGE evolution. In particular, the authors found in the HY scheme BR$^{[t=0]} = 3.28 \cdot 10^{-9}$ in Table 2 of their work. Adopting the same numerical input ($f_{B_s} = 227$ MeV, $\tau_{B_s} = 1.466$ ps^{-1}, $M_{B_s} = 5.36677$ GeV, $|V_{tb}V_{ts}^*| = 0.0405$, $m_\mu = 105.6584$ MeV $\Rightarrow \mathcal{N} = 4.48409 \cdot 10^5$) and Eq. (39), our result BR$^{[t=0]} = 3.13 \cdot 10^{-9}$ is about 5% lower, mainly due to the above mentioned approximations. Furthermore, the authors of Ref. [22] argued that NLO EW corrections in the HY scheme should be small and suggested a procedure, based on LO expressions, that lead to the preliminary value of BR$^{[t=0]} = 3.23 \cdot 10^{-9}$ (see Eq. (17) in Ref. [22]), which is closer to our result and deviates only by 3%. In particular it was suggested to use EW parameters α_e and s_W in the $\overline{\text{MS}}$ scheme at the scale $M_Z \approx 90$ GeV and the LO expression $c_{10}^{(11)} \sim Y_0(x_t)$ with $m_t(m_t)$ with an additional correction factor η_Y to account for higher-order QCD corrections from $c_{10}^{(21)}$. We find from Fig. 2, 3rd panel for the HY scheme, at $\mu_0 = 90$ GeV a deviation of about 1.5% between the LO result and the NLO EW one. We would like to close this comparison with the remark that the authors of Ref. [22] work at LO in the EW couplings allowing them to combine values of the input parameters which are dependent beyond the LO, where as in our case certain EW parameters, especially M_W and s_W, do depend on the input quantities of our choice in Eq. (16). As a consequence, a straightforward numerical comparison

is not possible, however, adopting the suggested procedure using our numerical values of dependent quantities we obtain a slightly larger value BR$^{[t=0]} = 3.24 \cdot 10^{-9}$ instead of $3.23 \cdot 10^{-9}$. For definiteness we give here our value $M_W^{\text{on-shell}} = (80.358 \pm 0.008)$ GeV obtained with [29] and our input values, which is close to the current measurement $M_W^{\text{PDG}} = (80.385 \pm 0.015)$ GeV [11]. The largest uncertainty is due to the variation of M_t^{pole} by ± 0.9 GeV. Moreover, we use the non-decoupling version for the $\overline{\text{MS}}$ renormalization of s_W^2 and obtain $s_W^2(M_Z) = 0.2317$ compared to the value 0.2314 compiled by the PDG [11].

V. CONCLUSIONS

We have calculated the next-to-leading (NLO) electroweak (EW) corrections to the Wilson coefficient $\mathcal{C}_{10}$ that governs the rare decays $B_q \to \ell^+\ell^-$ in the Standard Model. To assess the size of higher-order corrections, the numerical analysis has been performed within three different renormalization schemes of the involved EW parameters, described in Sec. II A, and two different normalizations of the effective Lagrangian, given in Eq. (6). The inclusion of NLO EW corrections strongly reduced the scheme dependences present at LO for all considered schemes. We identified the two schemes with the better convergence behavior and estimated the uncertainty from missing beyond NLO EW corrections to be about $\pm 0.3\%$ for $\mathcal{C}_{10}$. The first renormalization scheme is based on a new normalization [10] that eliminates the ratio $\alpha_e/s_W^2 \to G_F$ in favor of Fermi's constant. The second is based on the $\overline{\text{MS}}$ scheme for both quantities entering the ratio α_e/s_W^2 [21].

Apart from the NLO EW matching corrections to $\mathcal{C}_{10}$, we took into account the effects of the renormalization group running of $\mathcal{C}_{10}$ caused by operator mixing at higher order in QED in the effective theory. As we do not in-

clude QED corrections to the matrix elements of the relevant operators we estimated the remaining perturbative uncertainty due to the variation of the low-energy scale μ_b and found an about $\pm 0.2\%$ uncertainty for $\mathcal{C}_{10}$.

In the error budget, we do not include uncertainties due to higher-order QCD corrections, which are removed by the NNLO QCD calculation [36], nor parametric uncertainties of $\mathcal{C}_{10}$ and the branching ratio, which are discussed in detail in Ref. [37].

Our calculation removes an uncertainty of about $\pm 7\%$ at the level of the branching ratio and gives smaller values compared to the conjecture given in [22] by about $(3-4)\%$. We have estimated the final uncertainties due to beyond NLO EW corrections at the matching scale μ_0 and low-energy scale μ_b. The combination of both results in uncertainties of $\pm 0.5\%$ at the level of $\mathcal{C}_{10}$ and consequently $\pm 1\%$ on the branching ratio.

Appendix A: Details on the Matching Calculation

1. Operator Basis

Throughout, we use the same definition of the operators as in Ref. [23]. The RGE evolution from the matching scale μ_0 down to μ_b involves the operators mentioned in Sec. III, whereas here, we list only operators whose Wilson coefficients contribute to the matching of the NLO EW correction to $\mathcal{C}_{10}$ in Sec. II. They are the physical operator P_2 and the according evanescent operator E_2 [6] that mediate $b \to q\,\bar{c}c$

$$P_2 = (\bar{q}_L \gamma_\mu c_L)\,(\bar{c}_L \gamma^\mu b_L)\,, \tag{A1}$$

$$E_2 = (\bar{q}_L \gamma_{\mu\nu\rho} c_L)\,(\bar{c}_L \gamma^{\mu\nu\rho} b_L)\,, \tag{A2}$$

---

[6] Actually, E_2 does not contribute to the matching, but only because it does not mix in P_{10} at one-loop, i.e. $\hat{Z}^{(1)}_{E_2,10} = 0$.

as well as P_9, P_{10} and the according evanescent operators E_9 and E_{10} [24] that mediate $b \to q\,\ell^+\ell^-$

$$P_9 = (\bar{q}_L \gamma_\mu b_L) \sum_\ell (\bar{\ell}\gamma^\mu \ell)\,, \tag{A3}$$

$$P_{10} = (\bar{q}_L \gamma_\mu b_L) \sum_\ell (\bar{\ell}\gamma^\mu \gamma_5 \ell)\,, \tag{A4}$$

$$E_9 = (\bar{q}_L \gamma_{\mu\nu\rho} b_L) \sum_\ell (\bar{\ell}\gamma^{\mu\nu\rho}\ell) - 10 P_9 + 6 P_{10}\,, \tag{A5}$$

$$E_{10} = (\bar{q}_L \gamma_{\mu\nu\rho} b_L) \sum_\ell (\bar{\ell}\gamma^{\mu\nu\rho}\gamma_5 \ell) + 6 P_9 - 10 P_{10}\,. \tag{A6}$$

The evanescent operators vanish algebraically in $d = 4$ dimensions. Above $\gamma_{\mu\nu\rho} \equiv \gamma_\mu \gamma_\nu \gamma_\rho$ and $\gamma^{\mu\nu\rho} \equiv \gamma^\mu \gamma^\nu \gamma^\rho$. In our case, there are no equation-of-motion vanishing operators with a projection on $\langle P_{10}\rangle^{(0)}$ to contribute to the matching.

2. Details on the Standard Model Calculation

The two-loop EW SM calculation is very similar to the analogous calculation for the $K \to \pi\nu\bar{\nu}$ decays [21]. The calculation comprises of generating and calculating all two-loop topologies for the transition $b \to q\ell^+\ell^-$ (Fig. 1).

We perform two independent calculations, in the first we use `FeynArts` [38] to generate the topologies and a self-written `Mathematica` program to evaluate them and in the second `QGRAF` [39] and a self-written `FORM` [40] program, respectively.

By setting the external momenta and the masses of all fermions except for the top quark to zero all diagrams reduce to massive tadpoles with maximally three different masses. We reduce them to a few known master integrals using the recursion relations from Refs. [33, 41].

We work in dimensional regularization, which raises the question of how to treat γ_5 in $d \neq 4$ dimensions. The naive anticommutation relation (NDR) $\{\gamma_5, \gamma_\mu\} = 0$ can lead to algebraic inconsistencies in the evaluation of traces with γ_5's. Yet, the algebraically consistent definition of γ_5 by 't Hooft-Veltman (HV) [42] leads to spurious breaking of the axial-current Ward identities and as such requires the incorporation of symmetry-restoring finite counterterms. Diagrams that are free of algebraic inconsistencies in the NDR scheme yield the same finite result after the appropriate counterterms are added. This trivially holds for all diagrams free of internal fermion loops as well as for diagrams that involve traces with an even number of γ_5 matrices if the γ_5 matrices are eliminated through naive anticommutation from the relevant traces [43]. Since selfenergy diagrams involving a single axial coupling vanish, diagrams involving fermionic loops on bosonic propagators also correspond to the same finite expression in both schemes after appropriate renormalisation. Accordingly, special care has to be taken only for diagrams involving a fermion-triangle loop and coming with an odd number of γ_5 matrices. We use the HV prescription for these type of diagrams, since in particular

the diagram with three γ_5 matrices cannot be simply calculated in the NDR scheme. Here we note that the finite renormalization, which will restore the axial-anomaly relation of diagrams involving fermion traces, will drop out in our calculation after the sum over the complete set of standard model fermions is performed. This follows from the fact that Standard Model is anomaly free and can be understood by noting that e.g. the difference of the singlet and non-singlet counterterm in Ref. [43] has opposite sign for up-type and down-type quarks. Yet, one subtlety could arise from charged W and Goldstone bosons connecting the fermion-triangle diagram with the external fermion line. The axial couplings on the external line could in principle result in a spurious breaking of the axial-current Ward identity if treated in the HV scheme. Yet, only the 4-dimensional part of this coupling contributes if the fermion triangle contains an odd number of γ_5 matrices, since the corresponding diagrams are either finite after GIM or their traces vanish. Accordingly, we can safely use the HV scheme in these circumstances without the need of an extra finite renormalisation and calculate all other diagrams in the NDR scheme. The effective theory calculation does not involve fermion traces with γ_5 and for this reason can be performed completely in the NDR scheme.

In the SM, the renormalization scheme of the fermion fields $f = q, \ell$, i.e. quarks and leptons, is chosen such that the kinetic terms in the effective theory remain canonically normalized at NLO in EW interactions. As a consequence, Wilson coefficients of dimension three $b \to s$ mediating operators in the effective theory are zero. The bare SM fields, $f^{(0)}$, with flavor type i and of chirality-type a are renormalized

$$f_{i,a}^{(0)} = \left(\delta_{ij} + \frac{1}{2} Z_{ij}^a \right) f_{j,a} \qquad (A7)$$

with the help of the matrix-valued field renormalization constant Z^a. The latter is determined from one-loop $f \to f'$ two-point functions such that the matching relation for the fields in the SM and effective theory

$$f^{\text{full}} = f^{\text{eff}}, \qquad (A8)$$

holds, implying that tree-level matrix elements of operators, $\langle P_i \rangle^{(0)}$, are the same in the SM and effective theory amplitude, see Eqs. (17) and (24) respectively. For this purpose, the two-point functions are evaluated in an expansion up to first order in external momenta and masses over heavy masses. The heavy particle contributions yield finite parts to Z^a, whereas light particle contributions eventually drop out in the matching and thus may be discarded in the calculation. In addition, the flavor off-diagonal quark-field renormalization constant Z_{bq} is determined at two-loop level from the two-point function $b \to q$.

The counterterm of the CKM matrix is entirely determined by the field renormalization constants Z^L of the up- and down-quark fields. This renormalization prescription corresponds to a definition of the CKM elements

in the effective theory where the kinetic terms of all light quark fields are canonical.

Since we renormalize both the couplings α_e^{full} and α_e^{eff} of the full and effective theory, respectively, in the $\overline{\text{MS}}$ scheme, the α_e threshold corrections have to be included in the case of the single-G_F normalization. In the threshold corrections, $\Delta\alpha_e$,

$$\alpha_e^{\text{full}} = \alpha_e^{\text{eff}} \left[1 + \frac{\alpha_e^{\text{eff}}}{4\pi} \Delta\alpha_e \right],$$
$$\Delta\alpha_e = -\frac{2}{3} - 14 \ln\frac{\mu}{M_W} + \frac{32}{9}\ln\frac{\mu}{M_t} \qquad (A9)$$

the first two terms arise from the decoupling of the electroweak gauge bosons and the last term from the top quark at the scale μ. Since the definition of $\alpha_e(M_Z)$ in Tab. I compiled by the particle data group [11] already implies a decoupled top quark, we determine α_e^{eff} from $\alpha_e(M_Z)$ using only the gauge boson contribution and find $\alpha_e^{\text{eff}}(M_Z) = 1/127.751$ that we use in our numerical evaluations.

In order to match consistently, we apply Eq. (A9) to substitute the $\alpha_e^{\text{full}} \to \alpha_e^{\text{eff}}$, which affects the matching at next-to-leading order due to an additional contribution in the amplitude of the full theory from the lower order part in Eq. (18) (omitting here the subscript $A_{\text{full},10} \to A$)

$$\tilde\alpha_e^{\text{full}} A^{(1)} + \left(\tilde\alpha_e^{\text{full}}\right)^2 A^{(2)} =$$
$$\tilde\alpha_e^{\text{eff}} A^{(1)} + \left(\tilde\alpha_e^{\text{eff}}\right)^2 \left[A^{(2)} + \Delta\alpha_e A^{(1)} \right]. \qquad (A10)$$

3. Details on the Effective Theory Calculation

Before being able to evaluate the two-loop $b \to q\ell^+\ell^-$ amplitude in the effective theory we need to know all Wilson coefficients and renormalization constants appearing in Eq. (26). The tree-level contribution $\mathcal{C}_2^{(00)}$ and the one-loop results $\mathcal{C}_9^{(11)}$ and $\mathcal{C}_{10}^{(11)}$ are given in Ref. [33] including the $\mathcal{O}(\epsilon)$ terms for the latter two. Here we give in addition the Wilson coefficients of the two evanescent operators

$$c_{E_9}^{(11)} = c_{E_{10}}^{(11)} =$$
$$\frac{1}{16 s_W^2} \frac{x_t}{(x_t - 1)^2} \left(1 - x_t + \log x_t \right) + \mathcal{O}(\epsilon). \qquad (A11)$$

The $\mathcal{O}(\epsilon)$ terms of $c_{E_9}^{(11)}$ and $c_{E_{10}}^{(11)}$ do not contribute to the matching[7] as the mixing renormalization constants $\hat{Z}_{E_9,10}^{(1)}$ and $\hat{Z}_{E_{10},10}^{(1)}$ carry no divergent terms, only finite ones.

---

[7] The operator E_{10} does not contribute to the matching at all because $\hat{Z}_{E_{10},10}^{(1)} = 0$.

Having all relevant Wilson coefficients we return to the renormalization constants. We fix the field renormalization constants by extracting the UV poles of the appropriate photonic one-loop two-point functions in the five-flavor theory. The results are:

$$Z_i = 1 + \tilde{\alpha}_e\, Z_i^{(1)} + \dots \qquad (A12)$$

with

$$Z_d^{(1)} = -\frac{1}{9\epsilon}\,, \qquad\qquad Z_\ell^{(1)} = -\frac{1}{\epsilon}\,.$$

We proceed similarly for the constants governing the mixing of operators into P_{10}. We calculate the UV poles of all one-loop insertions of a given operator, project on the tree-level matrix element of P_{10} and absorb the left-over pole in the mixing renormalization constant.

For the case of physical operators mixing into physical ones we absorb only the divergences into the constants $\hat{Z}_{P,P}$. For evanescent operators this is not the case. Evanescent operators are unphysical in four dimensions and at each order in perturbation theory their operator basis needs to be extended. To ensure that the Wilson coefficients at a given fixed order are independent from the choice of evanescent operators in some higher order we include finite terms in $\hat{Z}_{E,P}$ and completely cancel the mixing of evanescent to physical operators.

We have calculated all contributing one-loop mixing renormalization constants including the mixing of evanescent to physical operators. The mixing of physical operators can also be extracted from the anomalous dimension matrices in Refs. [23, 24]. Here we report the relevant non-zero constants

$$\hat{Z}_{9,10}^{(1)} = -\frac{2}{\epsilon}\,, \qquad\qquad \hat{Z}_{E_9,10}^{(1)} = \frac{32}{3}\,. \qquad (A13)$$

We extract the $1/\epsilon$-part of the one two-loop renormalization constant we need from the corresponding anomalous dimension in Ref. [24] and calculated the $1/\epsilon^2$-term

$$\hat{Z}_{2,10}^{(2)} = \frac{4}{9\epsilon^2} - \frac{26}{27\epsilon}\,. \qquad (A14)$$

Appendix B: Details on the RGE

1. General

The dependence of the Wilson coefficients $\mathcal{C}_i$ on the renormalization scale μ is governed by the anomalous dimension matrix $\hat{\gamma}$

$$\mu\frac{d}{d\mu}\mathcal{C}_i(\mu) = \left[\hat{\gamma}^T(\mu)\right]_{ij}\mathcal{C}_j(\mu) \qquad (B1)$$

with the expansion in the couplings

$$\hat{\gamma}(\mu) = \sum_{\substack{m,n=0 \\ m+n\geq 1}} \tilde{\alpha}_s(\mu)^m \tilde{\alpha}_e(\mu)^n\, \hat{\gamma}_{(mn)}\,, \qquad (B2)$$

which is known up to and including relevant entries in $(mn) = (30)$ and (21). It has been solved as an expansion in terms of the small quantities [23]

$$\omega \equiv 2\beta_{00}^s\, \tilde{\alpha}_s(\mu_0), \qquad (B3)$$

$$\lambda \equiv \frac{\beta_{00}^e}{\beta_{00}^s}\frac{\tilde{\alpha}_e(\mu_0)}{\tilde{\alpha}_s(\mu_0)} = \frac{\beta_{00}^e}{\beta_{00}^s}\kappa(\mu_0) \qquad (B4)$$

in which case the evolution operator in Eq. (31) takes the form

$$U(\mu_b,\mu_0) = \sum_{m,n\geq 0}^{2} \omega^m \lambda^n\, U_{(mn)}\,, \qquad (B5)$$

excluding the term $(mn) = (22)$ that requires the knowledge of higher-order contributions to the anomalous dimension matrix. The $U_{(mn)}$ can be read off from Eq. (47) of Ref. [23], whereas the initial Wilson coefficients (in the single-G_F normalization) at the scale μ_0 have the expansion

$$c_i(\mu_0) = c_i^{(00)} + \omega\frac{c_i^{(10)}}{2\beta_{00}^s} + \omega^2\frac{c_i^{(20)}}{(2\beta_{00}^s)^2}$$
$$+ \omega\lambda\frac{c_i^{(11)}}{2\beta_{00}^e} + \omega^2\lambda\frac{c_i^{(21)}}{4\beta_{00}^e\beta_{00}^s} + \omega^2\lambda^2\frac{c_i^{(22)}}{(\beta_{00}^e)^2}\,. \qquad (B6)$$

The components $\mathcal{C}_{i,(mn)}$ of the downscaled Wilson coefficients in Eq. (32) are then obtained from the reexpansion of Eq. (31) in the new parameters $\tilde{\alpha}_s(\mu_b)$

$$\omega = 2\beta_{00}^s\, \eta\, \tilde{\alpha}_s(\mu_b)\,, \qquad (B7)$$

and $\kappa(\mu_b)$

$$\lambda = \frac{\beta_{00}^e}{\beta_{00}^s}\frac{\kappa(\mu_b)}{\eta}\Big[1 + \kappa(\mu_b)A_1(\eta)$$
$$+ \tilde{\alpha}_s(\mu_b)\kappa(\mu_b)A_2(\eta) + \mathcal{O}\left(\kappa^2,\, \tilde{\alpha}_s^2\right)\Big] \qquad (B8)$$

after inserting Eqs. (B5) and (B6). The coefficients $A_{1,2}(\eta)$ are given in Eq. (67) of Ref. [23].

2. Solution

Here the solution of the components $c_{10,(mn)}$ in Eq. (31) of the single-G_F normalization from Eq. (5) at the low scale μ_b are given in terms of $\eta = \alpha_s(\mu_0)/\alpha_s(\mu_b)$ and their initial components $c_i^{(mn)}$ in Eq. (12) at the matching scale μ_0. The derivation of the according results $\tilde{c}_{10,(mn)}$ for the quadratic-G_F normalization was given in Sec. III.

The numerical diagonalization of the leading-order anomalous dimension yields the exponents

$$a_i = (-2,\, -1,\, -0.899395,\, -0.521739,$$
$$-0.422989,\, 0.145649,\, 0.260870,\, 0.408619)\,. \qquad (B9)$$

The components read

i	1	2	3	4	5	6	7	8
b_i	0.00354	0.01223	−0.00977	−0.01070	−0.00572	0.00022	0.01137	−0.00117
$d_i^{(2a)}$	0	0	0.61602	0.44627	0.57472	0.08573	−0.48807	−0.24089
$d_i^{(2b)}$	−1.18162	0.22940	0.06522	−0.04380	−0.02201	−0.00316	−0.03366	−0.00414
$d_i^{(1)}$	0.01117	−0.03088	0.00411	0.00713	0.00478	0.00012	0.00379	−0.00023
$d_i^{(4)}$	−0.00799	−0.03666	0.06300	0	−0.01519	−0.00071	0	−0.00344
$e_i^{(1a)}$	0	0	−0.25941	−0.29751	−0.48014	0.04647	−0.16269	−0.04728
$e_i^{(1b)}$	1.13374	0.09381	−0.03041	0.00781	0.01838	−0.00138	−0.02259	0.00121
$e_i^{(4a)}$	0	0	−4.03683	0	1.52565	−0.27461	0	−0.70642
$e_i^{(4b)}$	3.38669	−0.10885	0.16283	0	0.06697	−0.01681	0	0.00137
$e_i^{(1)}$	0.01117	−0.03088	0.00411	0.00713	0.00478	0.00012	0.00379	−0.00023
$e_i^{(2)}$	0.00354	0.01223	−0.00977	−0.01070	−0.00572	0.00022	0.01137	−0.00117
$e_i^{(3)}$	0.02179	−0.12336	0.07870	0	0.01930	0.00873	0	−0.00516
$e_i^{(4)}$	−0.00799	−0.03666	0.06400	0	−0.01519	−0.00071	0	−0.00344
$e_i^{(5)}$	0.19550	−0.93249	0.37858	0	0.39909	0.05921	0	−0.09989
$e_i^{(6)}$	−0.17154	0.39616	0.01201	0	−0.19423	0.00357	0	−0.04597

TABLE II. Numerical values of b_i, $d_i^{(j)}$ and $e_i^{(j)}$ entering (B10).

$$c_{10,(11)} = c_{10}^{(11)}, \qquad c_{10,(21)} = \eta\, c_{10}^{(21)}, \qquad c_{10,(02)} = \sum_{i=1}^{8} b_i \eta^{a_i} c_2^{(00)},$$

$$
\begin{aligned}
c_{10,(12)} &= \sum_{i=1}^{8} \eta^{a_i+1}\Big[\left(d_i^{(2a)}\eta^{-1} + d_i^{(2b)} \right) c_2^{(00)} + d_i^{(1)} c_1^{(10)} + d_i^{(4)} c_4^{(10)} \Big] \\
&\quad - 0.11060\frac{\ln\eta}{\eta} c_2^{(00)} + \left(\eta^{-1} - 1\right)\left(0.26087\, c_9^{(11)} + 1.15942\, c_{10}^{(11)}\right),
\end{aligned}
\tag{B10}
$$

$$
\begin{aligned}
c_{10,(22)} &= \sum_{i=1}^{8} \eta^{a_i+2}\left[\left(e_i^{(1a)}\eta^{-1} + e_i^{(1b)}\right) c_1^{(10)} + \left(e_i^{(4a)}\eta^{-1} + e_i^{(4b)}\right) c_4^{(10)} + \sum_{j=1}^{6} e_i^{(j)} c_j^{(20)} \right] \\
&\quad + \left(0.27924\, c_1^{(10)} + 0.33157\, c_4^{(10)} + 2.35917\, c_9^{(11)} + 3.29679\, c_{10}^{(11)}\right)\ln\eta \\
&\quad + (1-\eta)\left(0.26087\, c_9^{(21)} + 1.15942\, c_{10}^{(21)}\right) + c_{10}^{(22)},
\end{aligned}
$$

with the coefficients b_i, $d_i^{(j)}$ and $e_i^{(j)}$ given in Tab. II.

Appendix C: Numerical study of $\mathcal{C}_{10}$ in OS-1 scheme

In this appendix we estimate higher-order corrections in the OS-1 scheme and supplement in this context the discussion of the OS-2 and HY schemes from Sec. IV. For this purpose, we proceed as in Fig. 3 and Fig. 4 and vary the matching scale μ_0, which allows to estimate higher-order QCD corrections via the dependence on the running top-quark mass. The result is shown in Fig. 6 at NLO QCD and NLO (EW + QCD) order normalized to the OS-2 result at the respective orders. To understand the different μ_0 dependence of the NLO QCD result for
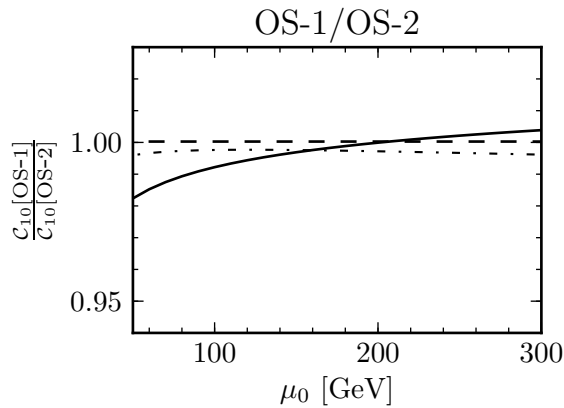
FIG. 6. The μ_0 dependence of the ratio of the Wilson coefficient $\mathcal{C}_{10}(\mu_b = 5\,\mathrm{GeV})$ in OS-1 and OS-2 schemes. The LO and NLO QCD result coincide (dashed). The full μ_0 dependence of NLO (QCD + EW) (solid) and partial μ_0 dependence for fixed $m_t(160\,\mathrm{GeV})$ in the s_W-on-shell counterterm (dashed dotted).

the OS-1 and OS-2 schemes, we remind that they involve different normalizations (see Eq. (7)), which bear a μ_0 dependence due to their m_t dependence when determining values of $M_W^{\text{on-shell}}$ and consequently $s_W^{\text{on-shell}}$, see Eq. (19) and the input in Eq. (16). As mentioned in Sec. II A, we calculate $M_W^{\text{on-shell}}$ with the aid of the result in Ref. [29], which incorporates various higher-order corrections that contribute beyond the NLO EW calculation of $\mathcal{C}_{10}$ performed in this work, especially those that require the choice of a particular renormalization scheme for the top-quark mass. Throughout we use the pole top mass as numerical input as in Ref. [29].

At NLO (EW + QCD) the OS-1 scheme exhibits a very different μ_0 dependence with respect to OS-2 and HY schemes, which is increased compared to NLO QCD. The main reason being the large EW two-loop correction to $c_{10}^{(22)}$ from the s_W-on-shell counterterm as already mentioned in connection with Fig. 2. The counterterm has a strong top-quark-mass dependence. To illustrate the latter, we present in Fig. 6 additionally the NLO (EW + QCD) result (dashed-dotted line) when keeping the scale of the running top-quark mass in the counterterm contribution fixed at $\mu_0 = 160$ GeV. Hence, the large shift caused by the electroweak two-loop correction in the OS-1 scheme is accompanied with an artificially large top-quark-mass dependence. As a consequence we do not consider the OS-1 scheme in our estimate of higher-order uncertainties. It would increase the estimate due to μ_0 variation of about $\pm 0.3\%$ given in Sec. IV to about $+0.4\%$ and -1.7%.

[1] R. Aaij *et al.* (LHCb Collaboration), Phys.Rev.Lett. **110**, 021801 (2013), arXiv:1211.2674 [hep-ex].
[2] R. Aaij *et al.* (LHCb collaboration), Phys.Rev.Lett. **111**, 101805 (2013), arXiv:1307.5024 [hep-ex].
[3] S. Chatrchyan *et al.* (CMS Collaboration), Phys.Rev.Lett. **111**, 101804 (2013), arXiv:1307.5025 [hep-ex].
[4] K. De Bruyn, R. Fleischer, R. Knegjens, P. Koppenburg, M. Merk, *et al.*, Phys.Rev.Lett. **109**, 041801 (2012), arXiv:1204.1737 [hep-ph].
[5] G. Raven (LHCb Collaboration), (2012), arXiv:1212.4140 [hep-ex].
[6] R. Aaij *et al.* (LHCb Collaboration), Phys.Lett. **B713**, 378 (2012), arXiv:1204.5675 [hep-ex].
[7] R. Aaij *et al.* (LHCb Collaboration), Phys.Rev.Lett. **108**, 241801 (2012), arXiv:1202.4717 [hep-ex].
[8] R. Aaij *et al.* (LHCb Collaboration), Eur.Phys.J. **C73**, 2373 (2013), arXiv:1208.3355 [hep-ex].
[9] T. Inami and C. Lim, Prog.Theor.Phys. **65**, 297 (1981).
[10] M. Misiak, (2011), arXiv:1112.5978 [hep-ph].
[11] J. Beringer *et al.* (Particle Data Group), Phys.Rev. **D86**, 010001 (2012).
[12] C. McNeile, C. Davies, E. Follana, K. Hornbostel, and G. Lepage, Phys.Rev. **D85**, 031503 (2012), arXiv:1110.4510 [hep-lat].
[13] A. Bazavov *et al.* (Fermilab Lattice Collaboration, MILC Collaboration), Phys.Rev. **D85**, 114506 (2012), arXiv:1112.3051 [hep-lat].
[14] H. Na, C. J. Monahan, C. T. Davies, R. Horgan, G. P. Lepage, *et al.*, Phys.Rev. **D86**, 034506 (2012), arXiv:1202.4914 [hep-lat].
[15] R. Dowdall, C. Davies, R. Horgan, C. Monahan, and J. Shigemitsu (HPQCD Collaboration), Phys.Rev.Lett. **110**, 222003 (2013), arXiv:1302.2644 [hep-lat].
[16] A. J. Buras, R. Fleischer, J. Girrbach, and R. Knegjens, JHEP **1307**, 77 (2013), arXiv:1303.3820 [hep-ph].
[17] G. Buchalla and A. J. Buras, Nucl.Phys. **B398**, 285 (1993).
[18] G. Buchalla and A. J. Buras, Nucl.Phys. **B400**, 225 (1993).
[19] M. Misiak and J. Urban, Phys.Lett. **B451**, 161 (1999), arXiv:hep-ph/9901278 [hep-ph].
[20] G. Buchalla and A. J. Buras, Nucl.Phys. **B548**, 309 (1999), arXiv:hep-ph/9901288 [hep-ph].
[21] J. Brod, M. Gorbahn, and E. Stamou, Phys.Rev. **D83**, 034030 (2011), arXiv:1009.0947 [hep-ph].
[22] A. J. Buras, J. Girrbach, D. Guadagnoli, and G. Isidori, Eur.Phys.J. **C72**, 2172 (2012), arXiv:1208.0934 [hep-ph].
[23] T. Huber, E. Lunghi, M. Misiak, and D. Wyler, Nucl.Phys. **B740**, 105 (2006), arXiv:hep-ph/0512066 [hep-ph].
[24] C. Bobeth, P. Gambino, M. Gorbahn, and U. Haisch, JHEP **0404**, 071 (2004), arXiv:hep-ph/0312090 [hep-ph].
[25] Tevatron-Electroweak-Working-Group (CDF Collaboration, D0 Collaboration), (2011), arXiv:1107.5255 [hep-ex].
[26] T. Aaltonen *et al.* (CDF Collaboration, D0 Collaboration), Phys.Rev. **D86**, 092003 (2012), arXiv:1207.1069

[hep-ex].

[27] G. Aad *et al.* (ATLAS Collaboration), Phys.Lett. **B716**, 1 (2012), arXiv:1207.7214 [hep-ex].

[28] S. Chatrchyan *et al.* (CMS Collaboration), Phys.Lett. **B716**, 30 (2012), arXiv:1207.7235 [hep-ex].

[29] M. Awramik, M. Czakon, A. Freitas, and G. Weiglein, Phys.Rev. **D69**, 053006 (2004), arXiv:hep-ph/0311148 [hep-ph].

[30] F. Jegerlehner, M. Y. Kalmykov, and O. Veretin, Nucl.Phys. **B641**, 285 (2002), arXiv:hep-ph/0105304 [hep-ph].

[31] F. Jegerlehner, M. Y. Kalmykov, and O. Veretin, Nucl.Phys. **B658**, 49 (2003), arXiv:hep-ph/0212319 [hep-ph].

[32] J. Fleischer and F. Jegerlehner, Phys.Rev. **D23**, 2001 (1981).

[33] C. Bobeth, M. Misiak, and J. Urban, Nucl.Phys. **B574**, 291 (2000), arXiv:hep-ph/9910220 [hep-ph].

[34] G. Buchalla and A. J. Buras, Phys.Rev. **D57**, 216 (1998), arXiv:hep-ph/9707243 [hep-ph].

[35] J. Fleischer, O. Tarasov, and F. Jegerlehner, Phys.Rev. **D51**, 3820 (1995).

[36] T. Hermann, M. Misiak, and M. Steinhauser, (2013), arXiv:1311.1347 [hep-ph].

[37] C. Bobeth, M. Gorbahn, T. Hermann, M. Misiak, E. Stamou, *et al.*, (2013), arXiv:1311.0903 [hep-ph].

[38] T. Hahn, Comput.Phys.Commun. **140**, 418 (2001), arXiv:hep-ph/0012260 [hep-ph].

[39] P. Nogueira, J.Comput.Phys. **105**, 279 (1993).

[40] J. Kuipers, T. Ueda, J. Vermaseren, and J. Vollinga, Comput.Phys.Commun. **184**, 1453 (2013), arXiv:1203.6543 [cs.SC].

[41] A. I. Davydychev and J. Tausk, Nucl.Phys. **B397**, 123 (1993).

[42] G. 't Hooft and M. Veltman, Nucl.Phys. **B44**, 189 (1972).

[43] S. Larin, Phys.Lett. **B303**, 113 (1993), arXiv:hep-ph/9302240 [hep-ph].